

Analysis of Ringdown Overtones in GW150914

Roberto Cotesta,¹ Gregorio Carullo,^{2,3,4} Emanuele Berti,¹ and Vitor Cardoso^{5,6}

¹*Department of Physics and Astronomy, Johns Hopkins University,
3400 N. Charles Street, Baltimore, Maryland, 21218, USA*

²*Dipartimento di Fisica “Enrico Fermi”, Università di Pisa, Pisa I-56127, Italy*

³*INFN sezione di Pisa, Pisa I-56127, Italy*

⁴*Theoretisch-Physikalisches Institut, Friedrich-Schiller-Universität Jena, Fröbelstieg 1, 07743 Jena, Germany*

⁵*CENTRA, Departamento de Física, Instituto Superior Técnico – IST,*

Universidade de Lisboa – UL, Avenida Rovisco Pais 1, 1049-001 Lisboa, Portugal

⁶*Niels Bohr International Academy, Niels Bohr Institute, Blegdamsvej 17, 2100 Copenhagen, Denmark*

(Dated: September 13, 2022)

We analyze GW150914 post-merger data to understand if ringdown overtone detection claims are robust. We find no evidence in favor of an overtone in the data after the waveform peak. Around the peak, the Bayes factor does not indicate the presence of an overtone, while the support for a nonzero amplitude is sensitive to changes in the starting time much smaller than the overtone damping time. This suggests that claims of an overtone detection are noise-dominated. We perform GW150914-like injections in neighboring segments of the real detector noise, and we show that noise can indeed induce artificial evidence for an overtone.

Introduction. Since the first detection of gravitational waves (GWs) from a binary black hole (BH) merger, GW150914 [1], the LIGO-Virgo-KAGRA (LVK) Collaboration [2–4] reported 90 events with a probability of astrophysical origin $p_{\text{astro}} > 0.5$ during the first three observing runs [5–8]. These GW signals, combined with those detected by independent groups [9–13], have broadened our understanding of cosmology [14], the astrophysics of compact objects [15], matter at supranuclear densities [16], and general relativity (GR) in the strong-field regime [17].

Among the numerous tests of GR proposed over the years, BH spectroscopy with the so-called “ringdown” relaxation phase following the merger presents unique opportunities to characterize the remnant as a Kerr BH. In linearized GR, the two GW polarizations $h_{+, \times}$ can be decomposed as $h_{+} - ih_{\times} \equiv \sum_{\ell m} h_{\ell m}(t) {}_{-2}Y_{\ell m}(t, \phi)$, where the (spin-weighted) spherical harmonics ${}_{-2}Y_{\ell m}(t, \phi)$ depend on two angles that characterize the direction from the source to the observer. Each multipolar component is a superposition of damped exponentials known as quasinormal modes (QNMs):

$$h_{\ell m}(t) \equiv \sum_n A_{\ell mn} e^{i[-\omega_{\ell mn}(t-t_{\ell mn}^{\text{start}}) + \phi_{\ell mn}]} e^{-(t-t_{\ell mn}^{\text{start}})/\tau_{\ell mn}}, \quad (1)$$

where we ignored spherical-spheroidal mode-mixing between different corotating ℓ modes, and the contribution of counterrotating modes (a valid assumption for GW150914). In GR, the QNM frequencies $\omega_{\ell mn}$ and damping times $\tau_{\ell mn}$ depend only on the remnant BH’s mass M_f and spin a_f [18–24]. The QNM amplitudes $A_{\ell mn}$ and phases $\phi_{\ell mn}$ were unknown before the first numerical BH merger simulations, and early work on BH spectroscopy [23] had to rely on educated guesses [25]. We now know that radiation from a binary BH merger is dominated by the $\ell = |m| = 2$ component, while higher multipoles are subdominant [26, 27]. For fixed (ℓ, m) , the QNMs are sorted by the magnitude of $\tau_{\ell mn}$: the fundamental mode ($n = 0$) has the longest damping time, and

the integer n labels the so-called “overtones.”

It has long been known that including overtones improves the agreement between ringdown-only fits and the complete gravitational waveforms from perturbed BHs. This was first shown by direct integration of the perturbation equations sourced by infalling particles or collapsing matter [29–32] and then, more rigorously, using Green’s function techniques [33–37]. Overtones were shown to improve agreement with numerical simulations of collapse [38], head-on collisions [39] and quasicircular mergers [26] leading to BH formation, and their omission leads to significant biases in mass and spin estimates [40, 41]. However, standard QNM tests often relied only on fundamental modes for two main reasons: overtones are short-lived and difficult to confidently identify in the data [42], and it is unclear whether multiple overtones have physical meaning or they just happen to phenomenologically fit the nonlinear part of the merger signal [26, 27].

Recently, Ref. [43] showed that including overtones up to $n = 7$ in the ringdown model improves the agreement with numerical relativity simulations for all times beyond the time t_{peak} where $|h_{+}^2 + h_{\times}^2|$ has a maximum, claiming that this observation “implies that the spacetime is well described as a linearly perturbed BH with a fixed mass and spin as early as the peak.” Their study’s insistence on an intrinsically linear physical description spurred a sequence of additional investigations, both on the modeling and on the observational side [37, 44–53]. If higher overtones can indeed be measured by starting at the peak, the larger ringdown signal-to-noise ratio (SNR) would open the door to more precise tests of GR. This theoretical argument motivated a reanalysis of GW150914. Ref. [54] fitted the post-peak waveform with a QNM superposition including overtones, and claimed evidence for “at least one overtone [...] with 3.6σ confidence.” The claim seems at odds with Ref. [46] and with the subsequent LVK analysis [17], both reporting weak evidence (with a \log_{10} -Bayes factor of only ~ 0.6) in favor of the “overtone model” including both

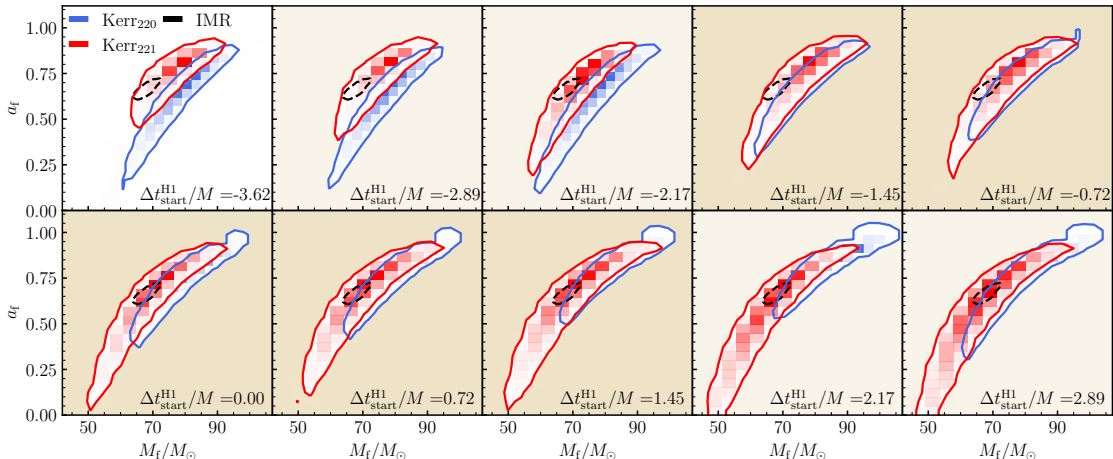


FIG. 1. Mass and spin of the remnant BH for GW150914. Each panel corresponds to a different value of $\Delta t_{\text{start}}^{\text{H1}} = t_{\text{start}}^{\text{H1}} - \bar{t}_{\text{peak}}^{\text{H1}}$, quoted in units of M . All $\Delta t_{\text{start}}^{\text{H1}}$ values used in panels with dark (light) gold backgrounds are consistent with the median of the $t_{\text{peak}}^{\text{H1}}$ distribution at 1σ (2σ). In each panel, dashed black, solid red, and solid blue contours correspond to 90% credible level in the BH parameters measured using the full IMR [28], Kerr₂₂₁, and Kerr₂₂₀ models, respectively.

$n = 0$ and $n = 1$ (henceforth Kerr₂₂₁) relative to the model including only $n = 0$ (henceforth Kerr₂₂₀).

In this paper we ask whether overtone detection claims in GW150914 data are robust. We use geometrical units $G = c = 1$, restoring physical units when needed, and we always quote redshifted BH masses as measured in a geocentric reference frame.

Methods. The $\ell = |m| = 2$ multipole is largely dominant in GW150914 [17, 55], so we can ignore higher multipoles and mode-mixing contributions in the general waveform model (1). The system does not show evidence for antialigned progenitor spins (and more generally, for any non-zero spin), so counterrotating modes can be safely ignored [17, 56]. We make several assumptions to match as closely as possible the analysis of Ref. [54]. First, we include only one or two QNMs ($n = 0, 1$) and assume that all overtones start at the same time $t_{\ell mn}^{\text{start}} = t_{\text{start}}$. We fix $(\iota, \phi) = (\pi, 0)$ rad, since in our model these parameters are strongly degenerate with the free overtone amplitudes and phases, respectively. Since there is no evidence for misaligned spins in GW150914, we also assume that the waveform amplitudes satisfy $h_{\ell m} = h_{\ell -m}^*$, a good approximation when the progenitor spins are nearly aligned with the orbital angular momentum of the binary. The strain measured by GW detectors is $h_{\text{D}}(t) = F_+ h_+ + F_\times h_\times$, where the detector pattern functions $F_{+,\times}(\alpha, \delta, \psi)$ depend on the right ascension, declination and polarization angles α , δ and ψ [57]. Following Ref. [54] we set $(\alpha, \delta, \psi) = (1.95, -1.27, 0.82)$ rad. We fix $t_{\text{start}}^{\text{H1}}$ in the Hanford detector and compute the starting time in the Livingston detector using a fixed time delay determined from the sky position parameters listed above. We assume flat priors on all free parameters in the ranges $M_f \in [20, 200] M_\odot$, $a_f \in [0, 0.99]$, $A_{22n} \in$

$[0, 5 \times 10^{-20}]$, $\phi_{22n} \in [0, 2\pi]$.

We analyze the ringdown signal using the Bayesian parameter estimation package `pyRing` [55, 58], employed by the LVK collaboration to perform ringdown-only tests of GR. The `pyRing` package relies on the nested sampling algorithm `cpnest` [59] (for additional details needed to reproduce our analysis, see the Software section), that allows us to compare alternative hypotheses by computing their relative Bayes factors. We use 4096 live points and 4096 maximum Markov Chain (MC) steps, which typically result in ~ 20000 independent samples at the end of each of our runs. We have tested the robustness of our results to sampling configurations by repeating the runs close to the peaktime using 10000 live points and MC steps, together with four different random seeds in the instantiations of the nested sampling. All the obtained results are consistently recovered under these changes of settings. The autocorrelation function (ACF) of the background noise was chosen to be as close as possible to the settings of Ref. [54]. The ACF was computed using a stretch of 64s of data starting at 1126257417s of GPS time (see the Software section for more details). We have verified that ACFs estimated using different data stretches close to the event do not significantly impact our conclusions, in agreement with the hypothesis of wide-sense stationarity of the noise. The data are appropriately cropped to avoid contamination from earlier stages of the coalescence [60], beginning from the starting time of the analysis and up to a duration of 0.1s. We analyze publicly available data from GWOSC [61] with a sampling rate of 16384 Hz (the maximum resolution available). This rate, larger than the rate of 2048 Hz used in Ref. [54], was chosen to minimize the impact of the time discretization. Repeating the analysis using a rate of 4096 Hz left our conclusions unaltered.

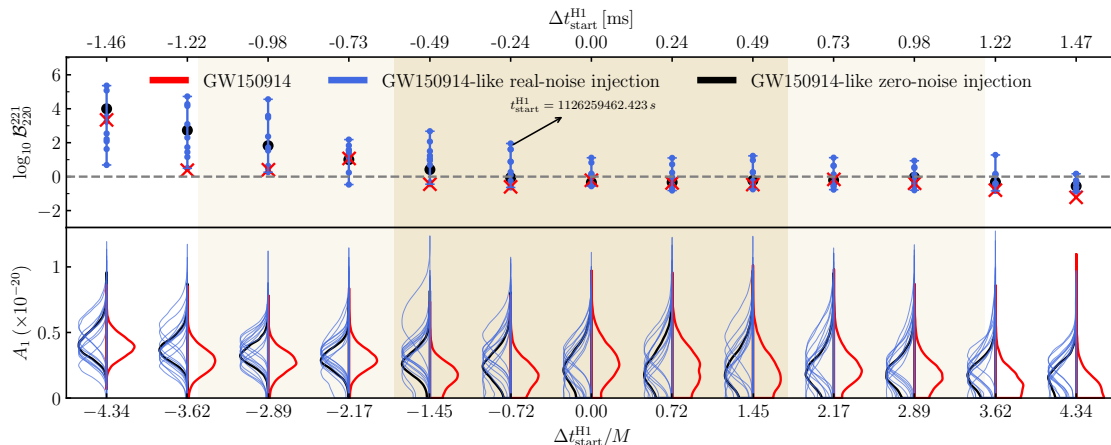


FIG. 2. *Top*: Log-Bayes factor ($\log_{10} \mathcal{B}_{220}^{221}$) between the Kerr₂₂₁ and Kerr₂₂₀ hypotheses as a function of $\Delta t_{\text{start}}^{\text{H1}} = t_{\text{start}}^{\text{H1}} - \bar{t}_{\text{peak}}^{\text{H1}}$. For the GW150914 signal (red crosses), $\bar{t}_{\text{peak}}^{\text{H1}}$ is the median of the posterior distribution from the full IMR analysis; dark (light) gold bands correspond to the 1σ (2σ) uncertainties on the median. For the GW150914-like injections (black), $t_{\text{peak}}^{\text{H1}}$ is computed from the simulation, and so it is known exactly. Black dots correspond to a GW150914-like injection in zero noise. The blue dots (and related “error bars”) are computed by repeating the analysis at each $t_{\text{start}}^{\text{H1}}$ under different realizations of the real detector noise close to the GW150914 trigger. *Bottom*: Amplitude of the overtone A_1 measured for different $t_{\text{start}}^{\text{H1}}$. The red (black) curves correspond to the measurement obtained from the GW150914 signal (GW150914-like injection in zero noise). The blue curves are the overtone amplitudes measured on the GW150914-like injection in real noise.

When investigating the consequences of slightly changing the analysis settings, we found that the choice of t_{start} (which has been set equal to t_{peak} according to the theoretical arguments in [43]) has by far the largest impact. The effect of varying ψ , ι is milder, and it will be discussed in a forthcoming paper [62], together with the impact of dropping the symmetry assumption on the amplitudes $h_{\ell m}$. Ref. [54] assumed $t_{\text{start}}^{\text{H1}} = t_{\text{peak}}^{\text{H1}} = 1126259462.423 \text{ s}$. However the value of $t_{\text{peak}}^{\text{H1}}$ must be estimated from the data, and as such it is uncertain. Fixing it to a specific value can induce systematic biases. We quantify this uncertainty by reconstructing $t_{\text{peak}}^{\text{H1}}$ using the posterior distributions of the parameters of GW150914 [63] obtained with the IMR waveform model SEOBNRv4 [64] (see the Supplemental Material for details). We check that the reconstruction is robust against waveform systematics by using also the IMRPhenomPv2 waveform model [65–67]. In the Hanford detector, the resulting posterior distribution has median $\bar{t}_{\text{peak}}^{\text{H1}} = 1126259462.42323 \text{ s}$ and standard deviation $\sigma = 0.00059 \text{ s}$. We will vary $t_{\text{start}}^{\text{H1}}$ within the $\pm 2\sigma$ interval of its posterior distribution.

Mass and spin estimates. In Fig. 1 we show the mass and spin of the GW150914 BH remnant estimated using the Kerr₂₂₀ (blue), Kerr₂₂₁ (red) and full IMR model [28] (dashed black) for 10 selected values of $\Delta t_{\text{start}}^{\text{H1}} \equiv t_{\text{start}}^{\text{H1}} - \bar{t}_{\text{peak}}^{\text{H1}}$. For $\Delta t_{\text{start}}^{\text{H1}}/M \geq -1.45$, the IMR posterior overlaps with both the Kerr₂₂₀ and Kerr₂₂₁ models at 90% credibility, although the Kerr₂₂₁ reconstruction peaks closer to the IMR estimate. The Kerr₂₂₁ model agrees much better than Kerr₂₂₀ with the IMR posterior especially when we start fitting before the peak ($\Delta t_{\text{start}}^{\text{H1}}/M \leq -2.17$), where such a fit is

not well motivated by the overtone model (see Fig. 1 of [43]). The starting time used in Ref. [54] corresponds to $\Delta t_{\text{start}}^{\text{H1}}/M = -0.72$ in Fig. 1. Note that the (M_f, a_f) measurements obtained with the Kerr₂₂₁ model overlap with the GR prediction even when $\Delta t_{\text{start}}^{\text{H1}}/M = -3.62$, outside of the 2σ confidence interval on the peak location. This is likely due to a combination of two effects: (i) since $\omega_{221} < \omega_{220}$, any overtone model naturally includes a low-frequency component, thus improving the fit to the low-frequency, pre-merger part of the signal; and (ii) the Kerr₂₂₁ model has a larger number of parameters than the Kerr₂₂₀ model, thus at low signal-to-noise ratios it can still fit the signal with the values of (M_f, a_f) determined by the late-time ringdown behavior.

Bayes factors. To quantify the evidence for the presence of an overtone in GW150914, we compare the hypotheses that the data can be described by the Kerr₂₂₁ vs. Kerr₂₂₀ models and compute the resulting Bayes factor, \mathcal{B}_{220}^{221} . In the top panel of Fig. 2 we show $\log_{10} \mathcal{B}_{220}^{221}$ (red crosses) for selected values of $\Delta t_{\text{start}}^{\text{H1}}$. In the bottom panel we show the posterior of the overtone amplitude $A_1 \equiv A_{221}$ for the Kerr₂₂₁ model (red curves). When $\Delta t_{\text{start}}^{\text{H1}}/M \geq -1.45$, there is no evidence for the overtone in the data ($\log_{10} \mathcal{B}_{220}^{221} < 0$), and the posterior distributions in the bottom panel have significant support for $A_1 = 0$, hence the Kerr₂₂₀ model is favored with respect to Kerr₂₂₁. We observe significant Bayesian evidence for the presence of the overtone ($\log_{10} \mathcal{B}_{220}^{221} > 2$) only for $\Delta t_{\text{start}}^{\text{H1}}/M \leq -4.34$, i.e., well outside of the nominal region of validity of the Kerr₂₂₁ model. For $\Delta t_{\text{start}}^{\text{H1}}/M = -0.72$, which corresponds to the $t_{\text{peak}}^{\text{H1}}$ value used in Ref. [54], we find that $\log_{10} \mathcal{B}_{220}^{221} = -0.60$, while the amplitude has large support for zero. At the peak time A_1 is maximum

away from zero, but there is still some support for zero amplitude. This may lead us to conclude that the overtone is measurable in this ringdown signal. However, both the Bayes factor and A_1 decrease for values of $\Delta t_{\text{start}}^{\text{H1}}$ located immediately before and after $\Delta t_{\text{start}}^{\text{H1}}/M = 0$. Now, the decay time for the overtone in question is $\tau_{221} \approx 1.3 \text{ ms} \approx 4M$. If the overtone were measurable, we would expect to find evidence for its presence when changing $t_{\text{start}}^{\text{H1}}$ by only $\sim 0.24 \text{ ms} \approx 0.72M$. Since this is not the case, we must consider the hypothesis that the (weak) evidence in favor of an overtone for $\Delta t_{\text{start}}^{\text{H1}}/M = 0$ could be driven by a noise fluctuation.

We test this hypothesis by using a synthetic signal (“injection”, in LVK jargon) obtained from a numerical solution of the Einstein equations consistent with the GW150914 signal [68] (see the Supplemental Material for details). In this case, $t_{\text{peak}}^{\text{H1}}$ is known exactly. We analyze the signal using different values of $t_{\text{start}}^{\text{H1}}$, such that $\Delta t_{\text{start}}^{\text{H1}}$ is consistent with the values used for the real signal. For each selected $\Delta t_{\text{start}}^{\text{H1}}$, we first perform the analysis described above in the case of the real signal, but we now set the noise realization to zero (“zero-noise” injection). The resulting parameter distributions will thus have an uncertainty consistent with the actual signal, while eliminating a possible shift of the posterior median due to noise fluctuations coincident with the signal. The values of $\log_{10} \mathcal{B}_{220}^{221}$ and A_1 obtained from this zero-noise injection are shown as black dots and black curves in the upper and lower panels of Fig. 2. When $\Delta t_{\text{start}}^{\text{H1}}/M = 0$ there is no evidence for an overtone ($\log_{10} \mathcal{B}_{220}^{221} = -0.21 < 0$) and A_1 has a large support for zero. For the zero-noise injection, the Bayes factor is greater than unity only when $\Delta t_{\text{start}}^{\text{H1}}/M \leq -1.45$, and it generally increases for lower values of $\Delta t_{\text{start}}^{\text{H1}}$, similarly to what happens for the real signal. The inferred amplitude of the overtone is consistent with the behavior observed for the Bayes factor, increasing for large negative values of $\Delta t_{\text{start}}^{\text{H1}}/M$.

To assess the impact of the detector noise on the measurement of $\log_{10} \mathcal{B}_{220}^{221}$ and A_1 , for each $\Delta t_{\text{start}}^{\text{H1}}$ we repeat the above analysis superposing the simulated signal to 10 different segments of the real detector noise close to the time of coalescence of GW150914 (see the Supplemental Material). The resulting Bayes factors are reported as blue dots and related “error bars” on $\log_{10} \mathcal{B}_{220}^{221}$: for each time $\Delta t_{\text{start}}^{\text{H1}}$, each dot corresponds to a specific noise realization, while the upper (lower) boundary of the error bar corresponds to the largest (smallest) $\log_{10} \mathcal{B}_{220}^{221}$ obtained from these injections. The blue curves in the lower panel are the posterior distributions of A_1 corresponding to the different noise realisations. These distributions (to be compared with the zero-noise black curves) quantify the impact of noise fluctuations on amplitude measurements. For $\Delta t_{\text{start}}^{\text{H1}}/M = 0$ and neighboring points, the negative values of $\log_{10} \mathcal{B}_{220}^{221}$ measured in the real signal are consistent with the negative values measured in the synthetic signal, if we account for the detector noise. The posterior distributions of A_1 shows that a “favorable” realization of the detector noise can lead to a measurement of A_1

that peaks away from zero (blue curves) – similarly to the actual signal (red curve) – although A_1 is consistent with zero in the case of the zero-noise injection (black curve). We conclude that the mild support for an overtone observed in the amplitude posterior (although never confirmed by the Bayesian evidence) is driven by the detector noise.

Discussion. We have performed a Bayesian data analysis of the GW150914 ringdown signal to understand if ringdown overtone detection claims are robust. We found no Bayesian evidence in favor of an overtone, nor a significant overtone amplitude measurement in GW150914 data after the waveform peak, where the inclusion of overtones in the ringdown model is expected to improve the agreement with numerical relativity simulations [41, 43]. There is mild support for a nonzero overtone amplitude in the data at the peak, but such support for $A_1 = 0$ is sensitive to changes in the starting time smaller than the overtone damping time. Most importantly, the Bayes factors never favor the detection of an overtone when varying the starting time within the 1σ credible region of the peak time reconstruction. This suggests that the detection is noise-dominated. We verified this hypothesis by performing GW150914-like injections in different segments of the real detector noise. These results differ from Ref. [60], where the impact of the real detector noise and peak time uncertainty were not considered.

For both real and synthetic signals, the evidence for the overtone and the uncertainty on the evidence (as measured by the blue “error bars”) generally increase for large negative values of $\Delta t_{\text{start}}^{\text{H1}}$. The overtone model is not expected to be valid in this region, but the larger number of degrees of freedom in the model can pick up a larger portion of the low-frequency, pre-merger signal power. At the same time, the evidence uncertainty grows dramatically – spanning up to four orders of magnitude for the earliest times shown in Fig. 2 – because the poorly constrained model can easily pick up noise fluctuations.

Our results reveal an intrinsic instability of the inference based on such a model. The instability may happen even in the absence of noise, because the mass and spin of the remnant extracted from numerical simulations vary significantly close to the peak of the radiation [27, 41, 69], and thus the assumption of a linear superposition of QNMs starting at the peak can lead to conceptual issues [44, 70]. As reported in Table I of Ref. [43], the amplitude of the fundamental mode is stable up to a few parts in 10^3 under the addition of overtones, but higher overtones have much less stable amplitudes: A_{221} varies by 8%, while A_{223} varies by more than 200%. This is inconsistent with our understanding of ringdown in the linearized regime, where (by definition) the QNM amplitudes should be constant [42, 45, 71, 72]. This phenomenon was also found in Ref. [73] over the full nonprecessing parameter space. In the absence of fitting errors for the overtone amplitudes, it is difficult to quantify how much of this variation can be ascribed to the current accuracy of numerical BH merger simulations, rather than

being due to a time-evolving background. This instability might also explain the incompatibility of the measurement $A_{221}/A_{220} \leq 2$ reported in [54, 60], compared to the predicted value $A_{221}/A_{220} \sim 4$ reported in Table I of [43].

A physical parametrization of the overtone amplitudes as a function of the progenitors parameters, similar to the one proposed in Refs. [42, 72] for the fundamental modes, may alleviate this problem. However parametrizations of nonspinning binary BH mergers find that such a “global” fit is not robust under variations of the starting time: see e.g. Figs. 3 and 4 of [45]. Overfitting issues are particularly difficult to address. For example, the accuracy of overtone models constructed using GR QNMs can be matched (or even surpassed) by adding “unphysical” low-frequency components corresponding to non-GR values of the frequency and damping time [44, 48]. Similar “pseudo-QNMs” were introduced in the context of effective-one-body models [74–76].

Our results for the Bayes factors are consistent with previous work. The large number of free parameters in the overtone model introduces an Occam penalty that must be balanced by large SNRs [46]. Even when modeling the overtone amplitudes as functions of the properties of the remnant progenitors, measuring several overtone frequencies may still be impractical: Fisher matrix estimates [45] suggest that it will be easier to obtain evidence for multiple modes using higher angular harmonics rather than overtones. These results are in contrast with the predictions of [60], which employed a different detection criterion. In future work we plan to investigate strategies for a robust modeling and measurement of higher overtones, and to revisit the BH spectroscopy horizon estimates of Refs. [77, 78].

Addendum. While this paper was under review, some of the authors of [54] revisited their original analysis, extending it to multiple times around the peak [79]. In the Supplemental Material we present a comparison with their publicly available data. Small differences between the two analyses (i.e., a different sampling algorithm, data sampling rate, and autocorrelation function estimation method) lead to moderately different overtone amplitudes, but we observe broad agreement with our main results. In particular, both sets of posteriors show significant railing against zero within the peak time uncertainty. This comparison does not point to any fundamental discrepancy between the two investigations, and our conclusions are unaltered.

A third independent reanalysis [80] made use of a standard frequency domain approach employed for most of the LVK parameter estimation runs, hence relying on extensively tested algorithms for sampling and estimation of the noise properties. The authors confirm our main conclusions. They report a “modest” (1.8σ) significance for the detection of an overtone, whereas Ref. [54] claimed “ 3.6σ confidence.” Perhaps more remarkably, the authors of Ref. [80] find a *negative* Bayes factor in favor of an

overtone when marginalizing over all of the relevant uncertainty in the peak strain time. Their work confirms that current detection claims depend on subtle data analysis details (such as, e.g., frequency-domain vs. time-domain estimation of the noise properties), which should not have any impact on a robust detection.

Acknowledgments. We are grateful to Max Isi for help in reproducing the analysis settings of Ref. [54], and to Walter Del Pozzo for valuable comments and suggestions. We thank Vishal Baibhav, Swetha Bhagwat, Juan Calderón Bustillo, Will Farr, Xisco Jiménez-Forteza, Danny Laghi, Lionel London, Paolo Pani, Saul Teukolsky and the Testing GR group of the LVK collaboration for stimulating discussions. R.C. and E.B. are supported by NSF Grants No. PHY-1912550, AST-2006538, PHY-090003 and PHY-20043, and NASA Grants No. 17-ATP17-0225, 19-ATP19-0051 and 20-LPS20-0011. This research project was conducted using computational resources at the Maryland Advanced Research Computing Center (MARCC). G.C. acknowledges support by the Della Riccia Foundation under an Early Career Scientist Fellowship. V.C. is a Villum Investigator supported by VILLUM FONDEN (grant no. 37766) and a DNRF Chair supported by the Danish National Research Foundation. This project has received funding from the European Union’s Horizon 2020 research and innovation programme under the Marie Skłodowska-Curie grant agreement No 101007855. We thank FCT for financial support through Project No. UIDB/00099/2020. We acknowledge financial support provided by FCT/Portugal through grants PTDC/MAT-APL/30043/2017 and PTDC/FIS-AST/7002/2020. The authors would like to acknowledge networking support by the GWverse COST Action CA16104, “Black holes, gravitational waves and fundamental physics”. This material is based upon work supported by NSF’s LIGO Laboratory which is a major facility fully funded by the National Science Foundation.

Software. LIGO-Virgo data are interfaced through GWpy [81]. Projections onto detectors are computed through LALSuite [82]. The ACFs are computed using the function `get_acf` of the `ringdown` package [60]. The `pyRing` package is publicly available at: <https://git.ligo.org/lscsoft/pyring>. We use the `cpnest` version 0.11.3 and the `pyRing` commit `2b96c569ff663bb71dabe6dae5f4177b79854340` on the master branch. To allow for reproducibility, we release the configuration file employed for our analysis at the reference time: see https://github.com/rcotesta/GW150914_ringdown. The other results on observational data can be reproduced by changing the starting time by the amount specified in Fig. 2, while we give the details needed to reproduce the injections in the Supplemental Material. This study made use of the open-software python packages: `corner`, `cython`, `h5py`, `matplotlib`, `numpy`, `scipy`, `seaborn` [83–89].

- [1] B. P. Abbott *et al.* (LIGO Scientific, Virgo), *Phys. Rev. Lett.* **116**, 061102 (2016), arXiv:1602.03837 [gr-qc].
- [2] J. Aasi *et al.* (LIGO Scientific), *Class. Quant. Grav.* **32**, 074001 (2015), arXiv:1411.4547 [gr-qc].
- [3] F. Acernese *et al.* (VIRGO), *Class. Quant. Grav.* **32**, 024001 (2015), arXiv:1408.3978 [gr-qc].
- [4] T. Akutsu *et al.* (KAGRA), *PTEP* **2021**, 05A101 (2021), arXiv:2005.05574 [physics.ins-det].
- [5] B. P. Abbott *et al.* (LIGO Scientific, Virgo), *Phys. Rev. X* **9**, 031040 (2019), arXiv:1811.12907 [astro-ph.HE].
- [6] R. Abbott *et al.* (LIGO Scientific, Virgo), *Phys. Rev. X* **11**, 021053 (2021), arXiv:2010.14527 [gr-qc].
- [7] R. Abbott *et al.* (LIGO Scientific, VIRGO), (2021), arXiv:2108.01045 [gr-qc].
- [8] R. Abbott *et al.* (LIGO Scientific, VIRGO, KAGRA), (2021), arXiv:2111.03606 [gr-qc].
- [9] A. H. Nitz, C. Capano, A. B. Nielsen, S. Reyes, R. White, D. A. Brown, and B. Krishnan, *Astrophys. J.* **872**, 195 (2019), arXiv:1811.01921 [gr-qc].
- [10] A. H. Nitz, T. Dent, G. S. Davies, S. Kumar, C. D. Capano, I. Harry, S. Mozzon, L. Nuttall, A. Lundgren, and M. Tápai, *Astrophys. J.* **891**, 123 (2020), arXiv:1910.05331 [astro-ph.HE].
- [11] A. H. Nitz, C. D. Capano, S. Kumar, Y.-F. Wang, S. Kastha, M. Schäfer, R. Dhurkunde, and M. Cabero, *Astrophys. J.* **922**, 76 (2021), arXiv:2105.09151 [astro-ph.HE].
- [12] T. Venumadhav, B. Zackay, J. Roulet, L. Dai, and M. Zaldarriaga, *Phys. Rev. D* **101**, 083030 (2020), arXiv:1904.07214 [astro-ph.HE].
- [13] B. Zackay, L. Dai, T. Venumadhav, J. Roulet, and M. Zaldarriaga, *Phys. Rev. D* **104**, 063030 (2021), arXiv:1910.09528 [astro-ph.HE].
- [14] R. Abbott *et al.* (LIGO Scientific, VIRGO, KAGRA), (2021), arXiv:2111.03604 [astro-ph.CO].
- [15] R. Abbott *et al.* (LIGO Scientific, VIRGO, KAGRA), (2021), arXiv:2111.03634 [astro-ph.HE].
- [16] K. Chatziioannou, *Gen. Rel. Grav.* **52**, 109 (2020), arXiv:2006.03168 [gr-qc].
- [17] R. Abbott *et al.* (LIGO Scientific, Virgo), *Phys. Rev. D* **103**, 122002 (2021), arXiv:2010.14529 [gr-qc].
- [18] W. H. Press, *Astrophys. J. Lett.* **170**, L105 (1971).
- [19] S. Chandrasekhar and S. L. Detweiler, *Proc. Roy. Soc. Lond. A* **344**, 441 (1975).
- [20] S. L. Detweiler, *Astrophys. J.* **239**, 292 (1980).
- [21] K. D. Kokkotas and B. G. Schmidt, *Living Rev. Rel.* **2**, 2 (1999), arXiv:gr-qc/9909058.
- [22] O. Dreyer, B. J. Kelly, B. Krishnan, L. S. Finn, D. Garrison, and R. Lopez-Aleman, *Class. Quant. Grav.* **21**, 787 (2004), arXiv:gr-qc/0309007.
- [23] E. Berti, V. Cardoso, and C. M. Will, *Phys. Rev. D* **73**, 064030 (2006), arXiv:gr-qc/0512160.
- [24] E. Berti, V. Cardoso, and A. O. Starinets, *Class. Quant. Grav.* **26**, 163001 (2009), arXiv:0905.2975 [gr-qc].
- [25] E. E. Flanagan and S. A. Hughes, *Phys. Rev. D* **57**, 4535 (1998), arXiv:gr-qc/9701039.
- [26] A. Buonanno, G. B. Cook, and F. Pretorius, *Phys. Rev. D* **75**, 124018 (2007), arXiv:gr-qc/0610122.
- [27] E. Berti, V. Cardoso, J. A. Gonzalez, U. Sperhake, M. Hannam, S. Husa, and B. Bruegmann, *Phys. Rev. D* **76**, 064034 (2007), arXiv:gr-qc/0703053.
- [28] B. P. Abbott *et al.* (LIGO Scientific, Virgo), *Phys. Rev. Lett.* **116**, 241102 (2016), arXiv:1602.03840 [gr-qc].
- [29] M. Davis, R. Ruffini, W. H. Press, and R. H. Price, *Phys. Rev. Lett.* **27**, 1466 (1971).
- [30] C. T. Cunningham, R. H. Price, and V. Moncrief, *Astrophys. J.* **224**, 643 (1978).
- [31] C. T. Cunningham, R. H. Price, and V. Moncrief, *Astrophys. J.* **230**, 870 (1979).
- [32] V. Ferrari and R. Ruffini, *Phys. Lett. B* **98**, 381 (1981).
- [33] E. W. Leaver, *Phys. Rev. D* **34**, 384 (1986).
- [34] N. Andersson, *Phys. Rev. D* **55**, 468 (1997), arXiv:gr-qc/9607064.
- [35] E. Berti and V. Cardoso, *Phys. Rev. D* **74**, 104020 (2006), arXiv:gr-qc/0605118.
- [36] Z. Zhang, E. Berti, and V. Cardoso, *Phys. Rev. D* **88**, 044018 (2013), arXiv:1305.4306 [gr-qc].
- [37] N. Oshita, (2021), arXiv:2109.09757 [gr-qc].
- [38] R. F. Stark and T. Piran, *Phys. Rev. Lett.* **55**, 891 (1985), [Erratum: *Phys.Rev.Lett.* 56, 97 (1986)].
- [39] P. Anninos, D. Hobill, E. Seidel, L. Smarr, and W.-M. Suen, *Phys. Rev. Lett.* **71**, 2851 (1993), arXiv:gr-qc/9309016.
- [40] E. Berti, J. Cardoso, V. Cardoso, and M. Cavaglia, *Phys. Rev. D* **76**, 104044 (2007), arXiv:0707.1202 [gr-qc].
- [41] V. Baibhav, E. Berti, V. Cardoso, and G. Khanna, *Phys. Rev. D* **97**, 044048 (2018), arXiv:1710.02156 [gr-qc].
- [42] L. London, D. Shoemaker, and J. Healy, *Phys. Rev. D* **90**, 124032 (2014), [Erratum: *Phys.Rev.D* 94, 069902 (2016)], arXiv:1404.3197 [gr-qc].
- [43] M. Giesler, M. Isi, M. A. Scheel, and S. Teukolsky, *Phys. Rev. X* **9**, 041060 (2019), arXiv:1903.08284 [gr-qc].
- [44] S. Bhagwat, X. J. Forteza, P. Pani, and V. Ferrari, *Phys. Rev. D* **101**, 044033 (2020), arXiv:1910.08708 [gr-qc].
- [45] X. Jiménez Forteza, S. Bhagwat, P. Pani, and V. Ferrari, *Phys. Rev. D* **102**, 044053 (2020), arXiv:2005.03260 [gr-qc].
- [46] J. C. Bustillo, P. D. Lasky, and E. Thrane, *Phys. Rev. D* **103**, 024041 (2021), arXiv:2010.01857 [gr-qc].
- [47] M. Okounkova, (2020), arXiv:2004.00671 [gr-qc].
- [48] P. Mourier, X. Jiménez Forteza, D. Pook-Kolb, B. Krishnan, and E. Schnetter, *Phys. Rev. D* **103**, 044054 (2021), arXiv:2010.15186 [gr-qc].
- [49] G. B. Cook, *Phys. Rev. D* **102**, 024027 (2020), arXiv:2004.08347 [gr-qc].
- [50] A. Dhani, *Phys. Rev. D* **103**, 104048 (2021), arXiv:2010.08602 [gr-qc].
- [51] A. Dhani and B. S. Sathyaprakash, (2021), arXiv:2107.14195 [gr-qc].
- [52] E. Finch and C. J. Moore, *Phys. Rev. D* **103**, 084048 (2021), arXiv:2102.07794 [gr-qc].
- [53] L. Magaña Zertuche *et al.*, (2021), arXiv:2110.15922 [gr-qc].
- [54] M. Isi, M. Giesler, W. M. Farr, M. A. Scheel, and S. A. Teukolsky, *Phys. Rev. Lett.* **123**, 111102 (2019), arXiv:1905.00869 [gr-qc].
- [55] G. Carullo, W. Del Pozzo, and J. Veitch, *Phys. Rev. D* **99**, 123029 (2019), [Erratum: *Phys.Rev.D* 100, 089903 (2019)], arXiv:1902.07527 [gr-qc].
- [56] X. Li, L. Sun, R. K. L. Lo, E. Payne, and Y. Chen, (2021), arXiv:2110.03116 [gr-qc].
- [57] M. Maggiore, *Gravitational Waves. Vol. 1: Theory and*

- Experiments*, Oxford Master Series in Physics (Oxford University Press, 2007).
- [58] G. Carullo, W. D. Pozzo, D. Laghi, M. Isi, and J. Veitch, “pyRing: a time-domain ringdown analysis python package,” <https://git.ligo.org/lscsoft/pyring>.
- [59] W. Del Pozzo and J. Veitch, “CPNest: an efficient python parallelizable nested sampling algorithm,” <https://github.com/johnveitch/cpnest>.
- [60] M. Isi and W. M. Farr, (2021), [arXiv:2107.05609](https://arxiv.org/abs/2107.05609) [gr-qc].
- [61] R. Abbott *et al.* (LIGO Scientific, Virgo), *SoftwareX* **13**, 100658 (2021), [arXiv:1912.11716](https://arxiv.org/abs/1912.11716) [gr-qc].
- [62] R. Cotesta, G. Carullo, E. Berti, and V. Cardoso, in preparation.
- [63] <https://dcc.ligo.org/LIGO-P1800370/public>.
- [64] A. Bohé *et al.*, *Phys. Rev. D* **95**, 044028 (2017), [arXiv:1611.03703](https://arxiv.org/abs/1611.03703) [gr-qc].
- [65] S. Husa, S. Khan, M. Hannam, M. Pürrer, F. Ohme, X. Jiménez Forteza, and A. Bohé, *Phys. Rev. D* **93**, 044006 (2016), [arXiv:1508.07250](https://arxiv.org/abs/1508.07250) [gr-qc].
- [66] S. Khan, S. Husa, M. Hannam, F. Ohme, M. Pürrer, X. Jiménez Forteza, and A. Bohé, *Phys. Rev. D* **93**, 044007 (2016), [arXiv:1508.07253](https://arxiv.org/abs/1508.07253) [gr-qc].
- [67] M. Hannam, P. Schmidt, A. Bohé, L. Haegel, S. Husa, F. Ohme, G. Pratten, and M. Pürrer, *Phys. Rev. Lett.* **113**, 151101 (2014), [arXiv:1308.3271](https://arxiv.org/abs/1308.3271) [gr-qc].
- [68] M. Boyle *et al.*, *Class. Quant. Grav.* **36**, 195006 (2019), [arXiv:1904.04831](https://arxiv.org/abs/1904.04831) [gr-qc].
- [69] L. Sberna, P. Bosch, W. E. East, S. R. Green, and L. Lehner, (2021), [arXiv:2112.11168](https://arxiv.org/abs/2112.11168) [gr-qc].
- [70] S. Bhagwat, M. Okounkova, S. W. Ballmer, D. A. Brown, M. Giesler, M. A. Scheel, and S. A. Teukolsky, *Phys. Rev. D* **97**, 104065 (2018), [arXiv:1711.00926](https://arxiv.org/abs/1711.00926) [gr-qc].
- [71] E. N. Dorband, E. Berti, P. Diener, E. Schnetter, and M. Tiglio, *Phys. Rev. D* **74**, 084028 (2006), [arXiv:gr-qc/0608091](https://arxiv.org/abs/gr-qc/0608091).
- [72] L. T. London, *Phys. Rev. D* **102**, 084052 (2020), [arXiv:1801.08208](https://arxiv.org/abs/1801.08208) [gr-qc].
- [73] X. J. Forteza and P. Mourier, *Phys. Rev. D* **104**, 124072 (2021), [arXiv:2107.11829](https://arxiv.org/abs/2107.11829) [gr-qc].
- [74] Y. Pan, A. Buonanno, M. Boyle, L. T. Buchman, L. E. Kidder, H. P. Pfeiffer, and M. A. Scheel, *Phys. Rev. D* **84**, 124052 (2011), [arXiv:1106.1021](https://arxiv.org/abs/1106.1021) [gr-qc].
- [75] T. Damour and A. Nagar, *Phys. Rev. D* **90**, 024054 (2014), [arXiv:1406.0401](https://arxiv.org/abs/1406.0401) [gr-qc].
- [76] R. Brito, A. Buonanno, and V. Raymond, *Phys. Rev. D* **98**, 084038 (2018), [arXiv:1805.00293](https://arxiv.org/abs/1805.00293) [gr-qc].
- [77] E. Berti, A. Sesana, E. Barausse, V. Cardoso, and K. Belczynski, *Phys. Rev. Lett.* **117**, 101102 (2016), [arXiv:1605.09286](https://arxiv.org/abs/1605.09286) [gr-qc].
- [78] I. Ota and C. Chirenti, (2021), [arXiv:2108.01774](https://arxiv.org/abs/2108.01774) [gr-qc].
- [79] M. Isi and W. M. Farr, (2022), [arXiv:2202.02941](https://arxiv.org/abs/2202.02941) [gr-qc].
- [80] E. Finch and C. J. Moore, (2022), [arXiv:2205.07809](https://arxiv.org/abs/2205.07809) [gr-qc].
- [81] D. Macleod *et al.*, “gwpv/gwpy: 2.0.3,” (2021).
- [82] LIGO Scientific Collaboration, “LIGO Algorithm Library - LALSuite,” free software (GPL) (2018).
- [83] D. Foreman-Mackey *et al.*, “dfm/corner.py: corner.py v.2.2.1,” (2021).
- [84] S. Behnel, R. Bradshaw, C. Citro, L. Dalcin, D. Seljebotn, and K. Smith, *Comput. Sci. Eng.* **13**, 31 (2011).
- [85] A. Collette, *Python and HDF5* (O’Reilly, 2013).
- [86] J. D. Hunter, *Comput. Sci. Eng.* **9**, 90 (2007).
- [87] C. R. Harris *et al.*, *Nature (London)* **585**, 357 (2020).
- [88] P. Virtanen, R. Gommers, T. E. Oliphant, M. Haberland, T. Reddy, D. Cournapeau, E. Burovski, P. Peterson, W. Weckesser, J. Bright, S. J. van der Walt, M. Brett, J. Wilson, K. Jarrod Millman, N. Mayorov, A. R. J. Nelson, E. Jones, R. Kern, E. Larson, C. Carey, I. Polat, Y. Feng, E. W. Moore, J. VanderPlas, D. Laxalde, J. Perktold, R. Cimrman, I. Henriksen, E. A. Quintero, C. R. Harris, A. M. Archibald, A. H. Ribeiro, F. Pedregosa, P. van Mulbregt, and S. . . Contributors, *Nature Methods* (2020).
- [89] M. Waskom *et al.*, “mwaskom/seaborn: v0.11.2 (august 2021),” (2021).

SUPPLEMENTAL MATERIAL

Details of the peak time reconstruction. The peak time in the Hanford detector is reconstructed by generating the h_+ , h_\times waveform polarizations in post-processing, using the LVK posterior samples [63], and computing the maximum of $h_+^2 + h_\times^2$. In the main text we use the peak time $t_{\text{start}}^{\text{H1}}$ reconstructed from the SEOBNRv4 model [64], but to quantify waveform systematics we have repeated the calculation using also the IMRPhenomPv2 model [65–67]. The resulting distribution has median $\bar{t}_{\text{peak,Pv2}}^{\text{H1}} = 1126259462.42371$ s and standard deviation $\sigma_{\text{Pv2}} = 0.00063$ s, i.e., it is shifted ~ 0.5 ms after the time inferred from SEOBNRv4. Thus, using the reconstruction from this alternative model would reinforce our conclusions. This difference also highlights the need to properly marginalize over the peak time when evaluating the robustness of ringdown analyses. As a conservative choice, the `pyRing` package internally approximates the analysis starting time as the point on the discretized time axis immediately after the t_{start} , specified as a float. The high sampling rate employed ensures that no issues due to this discretization arise.

Details of the injection study. In the injection study, we use the numerical relativity simulation `SXS:BBH:0305` from the public catalog [68] of the Simulating eXtreme Spacetimes (SXS) collaboration. This simulation was set up to reproduce the GW150914 signal. The black hole binary in the numerical waveform has mass ratio $q = 1.22$ and spins aligned with the orbital angular momentum, with dimensionless magnitudes $\chi_1 = 0.33$ and $\chi_2 = -0.44$. For the synthetic signal, we place the system at a luminosity distance of $D_L = 410$ Mpc and we use a redshifted total mass $M = 72M_\odot$, in agreement with the median values estimated by the LVK collaboration [28]. Finally, the simulated signal is superimposed to the real detector noise at times $[-30, -25, -20, -5, 5, 10, 15, 20, 25, 30]$ s with respect to the peak time $t_{\text{peak,inj}}^{\text{H1}} = 1126259472.423$ s, approximately 10 s after the coalescence time of GW150914. We use the same noise ACF used in the analysis of the GW150914 event.

Comparison with Ref. [79]. In Figs. 3 and 4 we compare our results to the publicly available posterior samples and Bayes factors from Ref. [79], where the authors of [54] reanalyzed GW150914. We find their results to be broadly consistent with ours, although we disagree on the conclu-

sions that can be drawn from these results. The green crosses in Fig. 3 (to be compared with Fig. 7 of [79]) show their estimates of the Bayes factors. The vertical lines in the top panel of Fig. 3 show two different estimates of t_{peak} from Ref. [79], obtained using either the IMRPhenomPv2 (solid) or SEOBNRv4ROM (dashed) waveforms: note that their own estimates of the peak time suggest that one should actually look for overtones at later times than our own estimate. The Bayes factors computed after the peak time do not significantly depart from zero in either of the two studies. In fact, the Bayes factors reported in Ref. [79] are always contained within the “error bars” determined by noise in Fig. 3. In conclusion, there is no robust statistical evidence for the presence of overtones. In our computation, we have taken care to restrict the prior as much as possible (without truncating the posterior distribution), hence the objection that the Bayes factors can be made arbitrary small by enlarging the prior range does not apply to this case.

As can be seen from Fig. 4, when allowing for uncertainties in the starting time reconstruction, the posterior distributions of the overtone amplitudes from Ref. [79] show significant railing against zero (the data used for this plot are the same data shown in Fig. 1 of [79], which however shows smoothed distributions on a different plotting scale). Given the statistical ($\sim 3.5M$ at 2σ credibility) and systematic ($\sim 1.5M$ after the reference time of Fig. 4, according to our analysis) uncertainties in the starting time reconstruction, the observed railing around the peak time does not allow us to conclude in favor of a confident detection of the overtone amplitude. We also note that it is not straightforward to draw conclusions from the ratio of the median and standard deviation (see [79]) when the posterior rails against zero, as it does at late times for this event.

One difference between our results and those of Ref. [79] concerns the tails of the posteriors: our overtone amplitude posteriors have generally larger uncertainty. Given the large number of live points we used, typically resulting in ~ 20000 posterior samples (compared to ~ 2000 of [79]), we are confident that our algorithm is correctly estimating the posterior tails. Let us also remark that while the authors of Ref. [79] show the results of a small number of injections, they do not systematically investigate the impact of the starting time on these injections. Our analysis implies that a systematic investigation of the effect of the starting time is critical to draw reliable conclusions.

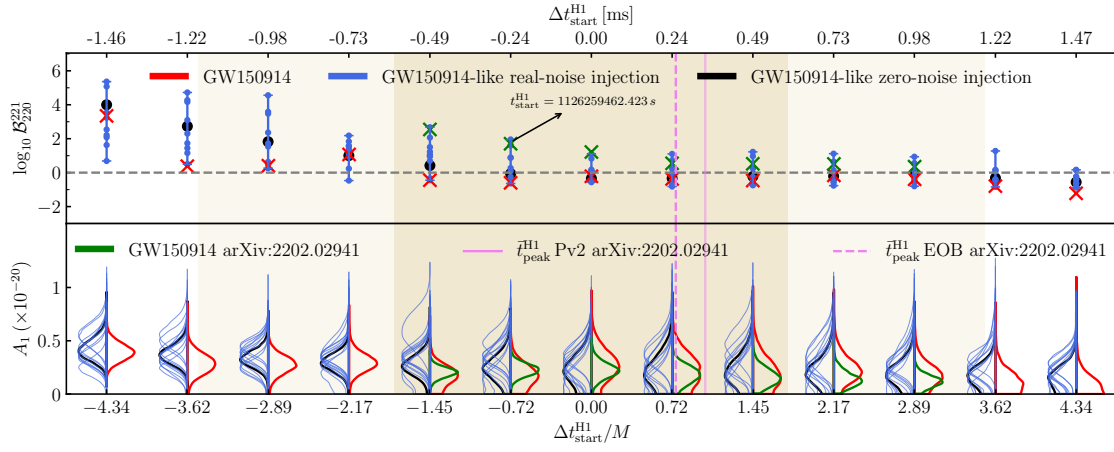


FIG. 3. Same as Fig. 2 in the main text, with the addition of (i) the Bayes factors estimated by Ref. [79] (green crosses in the top panel); (ii) the amplitude posteriors computed by Ref. [79] (shown in green in the bottom panel); and (iii) the estimates of t_{peak} by Ref. [79] obtained using either IMRPhenomPv2 (solid vertical line) or SEOBNRv4ROM (dashed vertical line).

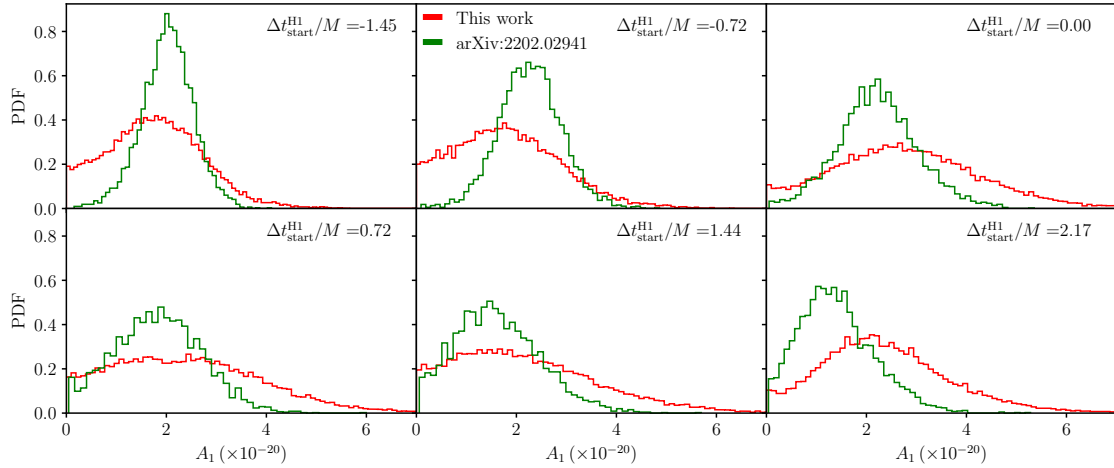


FIG. 4. Comparison of the posterior distributions of the overtone amplitude A_1 for a selected range of starting times close to the peak time estimate. Red histograms are our results (shown also in Fig. 3), while green histograms refer to the publicly available samples from Ref. [79].